NUMERICAL SIMULATION OF THE SINGLE-PHASE, COLD FLOW IN A DUMP COMBUSTOR

Francisco José de Souza, fjsouza@mecanica.ufu.br
Bruno Ribeiro Guimarães, brunoribeiroguimaraes@hotmail.com
Leonardo Vidigal Alves, lv_alves@hotmail.com
Federal University of Uberlandia
School of Mechanical Engineering
MFLAB - Laboratório de Mecânica dos Fluidos
Av. João Naves de Ávila, 2121
Uberlandia – Minas Gerais – Brazil

Abstract. *Highly swirling flows have proven difficult to predict with RANS (Reynolds-Averaged Navier Stokes) turbulence modeling. In swirl-based dump combustors, instabilities in the core flow might exist owing to phenomena like the precessing vortex core and vortex breakdown, depending on the swirl intensity. Although these unsteady phenomena can be successfully predicted by LES (Large-Eddy Simulation), as demonstrated in several publications, the inherent computational cost of such simulations becomes prohibitive for practical applications, since these devices normally operate at high Reynolds numbers. In this work, an attempt is made to check the limits of the applicability of the SST (Shear-Stress transport) turbulence model to the non-reacting, single-phase flow in a swirl-based combustion chamber. A laboratory-scale combustor is simulated at different swirl levels, and the average velocities and turbulence characteristics are compared to the measurements available at Reynolds number 125,000. Results for the nonswirling flow are satisfactory regarding the axial velocity, while the swirling velocity magnitude is overpredicted for a higher swirl number. Although successfully applied to strongly swirling cyclone flows, the empirical function to account for streamline curvature proposed by Spalart and Shur (1997) is also tested, unsuccessfully. Since this correction has been successfully applied to other swirling flows, it is believed that the inclusion of the swirler in the present model might positively affect the quality of the predictions.*

Keywords*: swirling flow, swirling dump combustor, SST turbulence model, curvature correction.*

1. INTRODUCTION

The combustor is one of the main components of a gas turbine engine, along with the compressor and the turbine. Despite the advances in understanding the phenomena taking place within combustion chambers and the combustion itself, a successful combustor design has been a challenge from the earliest gas turbines of Whittle and von Ohain (Langston and Opdyke, 1997). There are many requirements to be satisfied, some of which are conflicting, requiring design compromises to be made. Particularly for aircraft applications, the basic design requirements can be classified as follows ((Langston and Opdyke, 1997):

1 – high combustion efficiency at all operating conditions;
2 – low levels of unburned hydrocarbons and carbon monoxide low oxides of nitrogen at high power and no visible smoke;
3 – low pressure drop. Three to four percent is common;
4 – combustion must be stable under all operating conditions;
5 – consistent reliable ignition must be attained at very low temperatures, and at high altitudes;
6 - smooth combustion, with no pulsations or rough burning;
7 – a low temperature variation for good turbine life requirements;
8 – useful life (thousands of hours);
9 – length and diameter compatible with engine envelope (outside dimensions);
10 – design for minimum cost, repair and maintenance;
11 – minimum weight.

As main advantages, gas turbine engines are capable of producing large amounts of useful power for a relatively small size and weight, can be brought up to full-load (peak output) conditions in minutes and can utilize a wide variety of fuels, and as basic power supply, requires no coolant (e. g. water). As aeroderivative gas turbines are being increasingly used for base load electrical power generation, the effects of using different fuels (e.g. natural gas and Diesel fuel) must be understood, which in turn requires in-depth knowledge of the combustion process. As a natural step towards the prediction of the combustion, the fluid flow must be accurately calculated.

In this work, the non-reacting, single-phase flow within a laboratory combustion chamber, which mimics a gas turbine combustor, is simulated using CFD techniques. The experimental setup (Ahmed and Nejad, 1992) uses a swirler to vary the flow pattern and the swirl coefficient from 0 to 0.5. Results for average, second and third-order momentum components as well as turbulence quantities are available at several streamwise stations. The Reynolds number of the

experiments is 125,000, and therefore turbulence must be taken into account in the simulations. Ideally, Direct Numerical Simulation appears to be the ultimate choice, as it has no constraints regarding the turbulence features. Nevertheless, it is still too costly to be employed in this case. Large Eddy Simulations (LES) offer a good compromise between cost and accuracy, as the most energetic scales, which are also the most anisotropic, are directly resolved and the smallest ones are modeled. Although LES have proven to be reliable and accurate for many free-shear and wall-bounded flows, it is still costly at high Reynolds numbers because it should be, strictly speaking, equivalent to a DNS in the near-wall regions. Although previous works have shown that strongly swirling flows normally require higher-order closure RANS turbulence models, such as the Reynolds Stress Model, the applicability of the SST model to increasingly swirling flow is assessed. It can be concluded that the model performance for the nonswirling case is satisfactory while the numerical results considerably deviate from the experimental ones at swirl coefficient 0.4. The curvature correction proposed by Spalart and Shur (1997) is also experimented with, but the results display no improvement. Care has been taken to ensure that the solutions are mesh-independent in both cases.

2. DESCRIPTION OF THE EXPERIMENT

The combustion chamber investigated by Ahmed and Nejad (1992) is displayed in Fig. 1. Essentially, the air flow from the inlet pipe is forced into a swirler, which then imparts tangential momentum into the flow entering the combustor. The diameter of the inlet duct is 101.6 mm, while the diameter of the chamber is 152.4 mm. The total length of the combustion chamber is 2850 mm. LDA was used for measuring average velocities, statistical moments and turbulence data, which are available at the following stations: x/H=0.38, 1, 2, 3, 4, 5, 6, 8, 10, 12, 15 and 18. All these data are publicly available at the ERCOFTAC webpage. The Reynolds number based on the reference velocity 19.2 m/s is 125,000. At the temperature at which the experiments were run the air kinematic viscosity was 1.56 x 10^{-5} m^2/s.

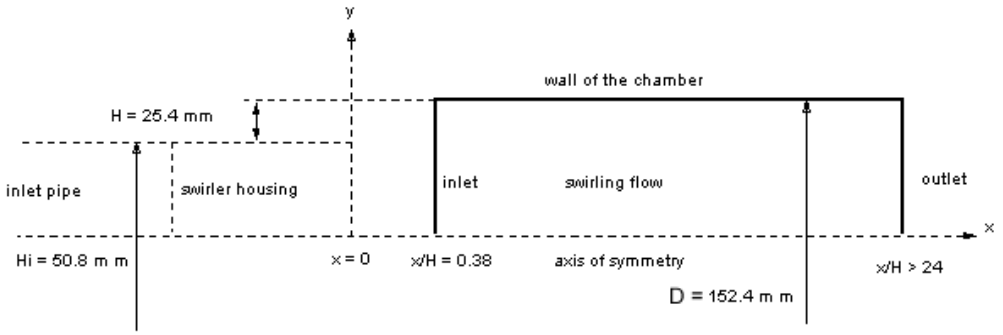

Figure 1. Details of the combustion chamber investigated (adapted from Ahmed and Nejad, 1992).

The swirl coefficient, defined as:

$$S = \int_0^R UWr^2\,dr \Big/ \int_0^R RU^2 r\,dr \tag{1}$$

can be varied in the experiments. Results for swirl coefficients ranging from 0 to 0.5 are also available at the ERCOFTAC site.

3. MATHEMATICAL MODEL AND NUMERICAL METHOD

The Reynolds-averaged Navier-Stokes equations are used to describe the cold flow in the combustor. The mass and momentum conservation can be written as:

$$\frac{\partial(\rho u_i)}{\partial x_i} = 0 \tag{2}$$

$$\frac{\partial}{\partial x_j}\left(\rho u_i u_j\right) = -\frac{\partial p}{\partial x_i} + \frac{\partial}{\partial x_j}\left[(\mu + \mu_t)\left(\frac{\partial u_i}{\partial x_j} + \frac{\partial u_j}{\partial x_i}\right)\right] \tag{3}$$

Because the Reynolds number is high, turbulence effects cannot be neglected. The SST model (Menter, 1993) is used, since it can cope with the turbulence effects in the core flow as well as in the near-wall region:

$$\frac{\partial \rho u_j k}{\partial x_j} = P_k - \beta^* \rho k\omega + \frac{\partial}{\partial x_j}\left[(\mu + \sigma_k \mu_t)\frac{\partial k}{\partial x_j}\right] \tag{4}$$

$$\frac{\partial \rho u_j \omega}{\partial x_j} = \gamma P_\omega - \beta \rho \omega^2 + \frac{\partial}{\partial x_j}\left[(\mu + \sigma_k \mu_t)\frac{\partial \omega}{\partial x_j}\right] + 2(1 - F_1)\rho\sigma_\omega \frac{1}{\omega}\frac{\partial k}{\partial x_j}\frac{\partial \omega}{\partial x_j} \tag{5}$$

$$\mu_t = \frac{a_1 \rho k}{\max(a_1 \omega, \Omega F_2)} \tag{6}$$

Ω is the magnitude of the vorticity tensor. The constants above and the production terms and blending functions F_1 and F_2 can be found in Menter (1993).

For the case with S=0.4, the curvature correction proposed by Spalart and Shur (1997) is also used in an effort to reduce the disparity between numerical results and experiments. Essentially, the production terms in Eqs. (4) and (5) are multiplied by an empirical function f_r, which includes the effect of the streamlines curvature in the production of turbulence kinetic energy and its specific dissipation rate:

$$f_r = max(min(f_{rotation}, 1.25), 0) \tag{7}$$

$$f_{rotation} = (1 + c_{r1})\frac{2r^*}{1 + r^*}[1 - c_{r3} tan^{-1}(c_{r2}\tilde{r})] - c_{r1} \tag{8}$$

$$r^* = \frac{S}{\Omega} \; and \; \tilde{r} = \Omega_{ij}^{cc}\frac{\Omega_{ik}}{\Omega}\frac{2}{\sqrt{D}} \tag{9}$$

$$where \quad \Omega_{ik}^{cc} = \frac{S_{jk}}{D}\frac{DS_{ij}}{Dt} \quad and \quad D = \max(S^2, 0.09\omega^2) \tag{10}$$

Constants c_{r1}, c_{r2} and c_{r3} take the values 1, 2 and 1, respectively.

The code used to solve the equations above is an in-house tool based on a cell-centered, finite-volume discretization on unstructured grids and is able to calculate flows within and over complex geometries. The transport equations (3), (4), and (5) can be cast in a general integral form for and arbitrary control volume:

$$\int_A \rho\phi\vec{V}.d\vec{A} = \int_A \Gamma \text{grad}\phi.d\vec{A} + \int_V S_\phi dV \tag{11}$$

Applying the equation above to element L, at the LHS of face *f*:

$$\sum_f J_f \phi_f = \sum_f \Gamma_f (grad\phi)_f.\vec{A}_f + (S_\phi \Delta V)_L \tag{12}$$

where J_f is the mass flow rate $(\rho_f \vec{V}_f.\vec{A}_f)$ through element face *f*, Γ_f the diffusion coefficient at that face, and the summations apply over the faces of element L. $\vec{A}_f$ is the normal area vector pointing outwards, that is, from element L to element R.

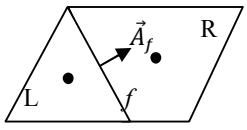

Figure 2. General control volume and nomenclature

The solver is pressure-based and velocity and pressure are coupled by the SIMPLE algorithm on unstructured meshes (Ferziger and Peric, 2002). For further details on the numerical method, the reader is referred to Mathur et al (1997) and Kim et al (1998). The gradients of the variables in each control volume are computed with the Gauss theorem. The face gradients, required in Eq. (11), are computed as averages of the elements gradients sharing that face. As for the advective terms, the second-order upwind scheme was used for the momentum, whereas the first-order upwind was used for the SST model equations. Because the speeds involved in the experiment are low, the flow was assumed to be incompressible and the energy conservation equation is not solved. An iterative procedure is then set in

which the 3 momentum equations are solved along with a Poisson-like equation for the pressure correction and the equations for the turbulence kinetic energy and its specific dissipation rate are solved. Convergence is declared when the residuals for the linear systems for u, v, w, k and ω and the pressure correction equation source term drop below 10^{-5}.

Figure 3 shows the first mesh used in the simulations, which contains approximately 282,000 hexahedra. It is important to emphasize that, since no geometrical information about the swirler is available, the experimental profile at x/H=0.38 was prescribed at the inlet boundary in the simulations. Basically, the experimental profile for the three Cartesian components, the turbulence kinetic energy and the specific kinetic energy dissipation rate along the combustor radius were interpolated to the inlet face centers. Because no wall-functions are employed (conversely, the equations are integrated all the way down to the walls), special care was taken to guarantee that the boundary layer is appropriately resolved and that y^+ in the elements adjacent to the walls are nearly 1. The flow is assumed to be fully developed at the outlet boundary, because the domain is long enough. From a numerical point of view, the velocity components and turbulence variables are extrapolated from the adjacent inner to the outlet face. In order to ensure mesh-independent solutions, a finer mesh simulation (483,000 elements) was run and the results were virtually identical to the ones shown in the next section. It is important to notice that the chamber section right downstream of the sudden expansion, at x/H=0, is not simulated, since there is no experimental information about it. Although this works when the profile is prescribed before the expansion, it might be argued that disregarding this length and the swirler geometry will have consequences on the results because of the influence of this part of the domain downstream.

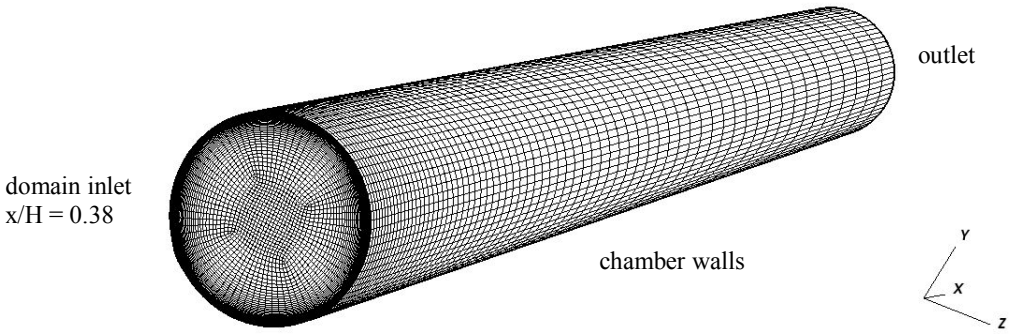

Figure 3. Mesh used in the simulations (nearly 282,000 hexahedra).

4. RESULTS AND DISCUSSION

4.1. Results for S=0

The nonswirling flow actually corresponds to a confined jet. Though wall-bounded, it displays the features normally observed in free shear jets, such as the high production of turbulence kinetic energy in the shear layer region and potential core decay, as can be seen in Figs. 4 and 5. It can also be seen that lateral recirculation zones are present up to x/H=8. This is a natural effect of the sudden expansion (dump), and is meant to promote stabilization of the flame after ignition as well as better reactant mixing.

Figures 6 to 14 present the results for the average velocity components for the nonswirling flow along the combustor chamber radius. The agreement between numerical and experimental results is fairly good for the streamwise velocity (U) in most stations. As for the spanwise velocity components, nonphysical spikes can be noticed in the experimental data, perhaps due to the inherent difficulty in measuring such small values in this case. Nevertheless, the order of magnitude is reasonably well predicted by the simulations. The inlet profiles, shown in Fig. 6, display a slight deviation from the experimental data at the centerline. While the numerical profile at this location should match exactly the experiments (the profile prescribed is interpolated to the faces of the inlet boundary), this discrepancy is due to the interpolation process and is believed not to affect the overall results of the simulation. Although the potential core of the inlet jet is underpredicted, particularly from station x/H=8 on, the axial centerline velocity decay is well captured, as can be seen in Figs 10 and 11.

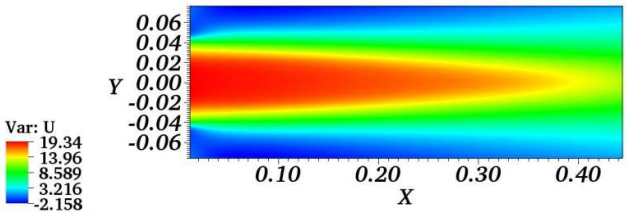

Figure 4. Contours of the streamwise velocity for the nonswirling flow.

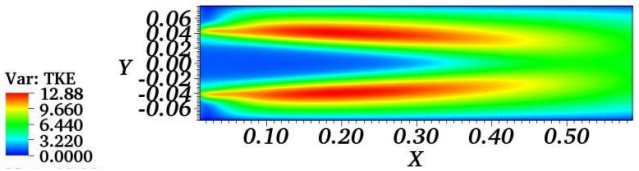

Figure 5. Contours of the turbulence kinetic energy for the nonswirling flow.

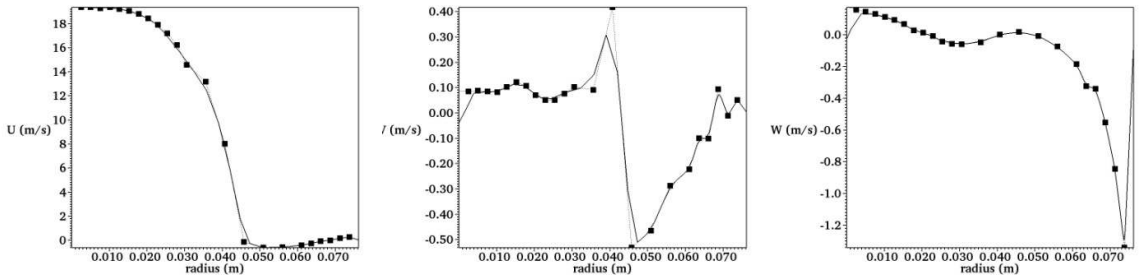

Figure 6. Results for the velocity components at x/H=0.38 (combustor inlet). Squares – experiment, Full line – numerical.

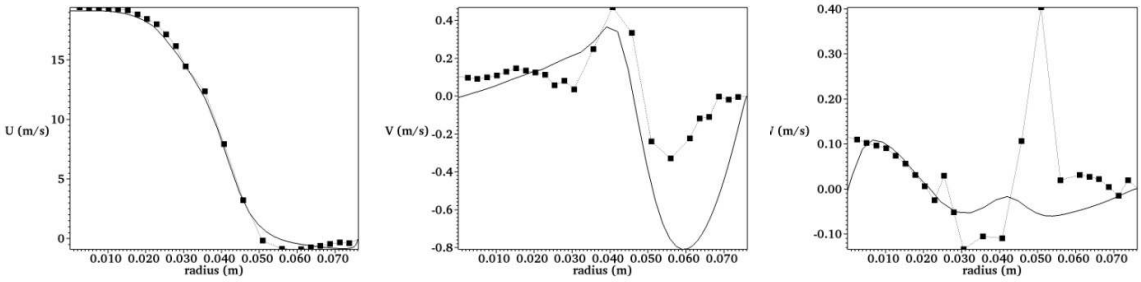

Figure 7. Results for the velocity components at x/H=1.0. Squares – experiment, Full line – numerical.

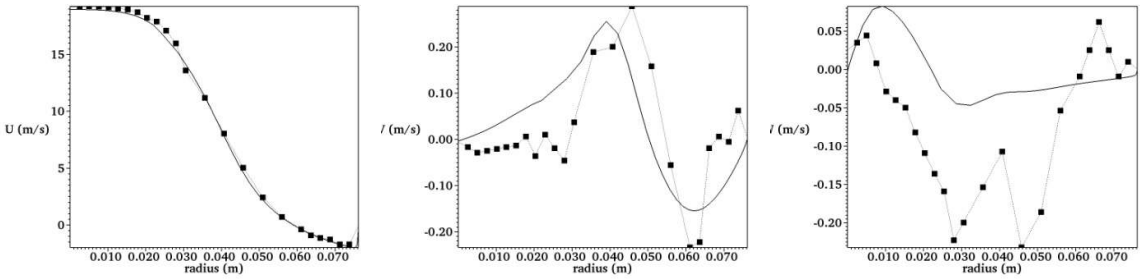

Figure 8. Results for the velocity components at x/H=2.0. Squares – experiment, Full line – numerical.

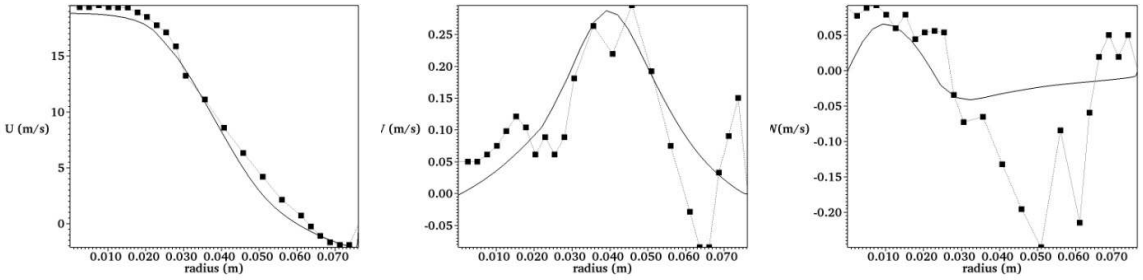

Figure 9. Results for the velocity components at x/H=3.0. Squares – experiment, Full line – numerical.

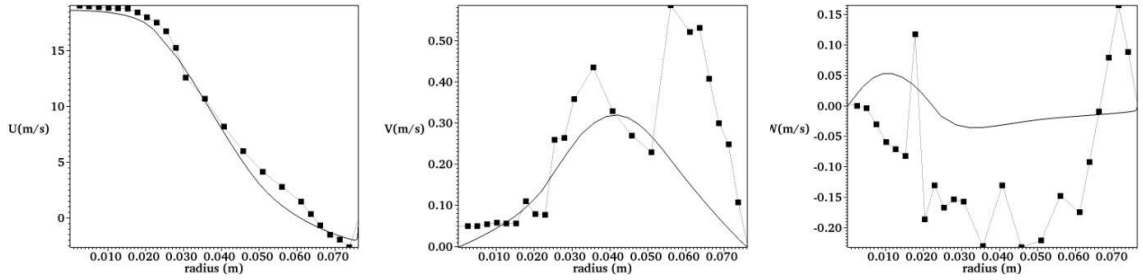

Figure 10. Results for the velocity components at x/H=4.0. Squares – experiment, Full line – numerical.

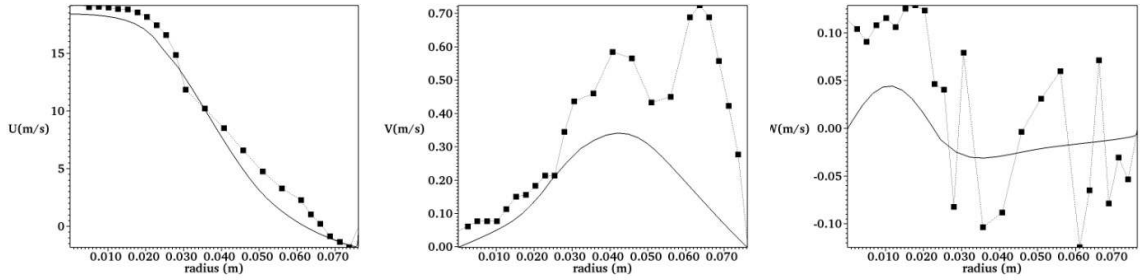

Figure 11. Results for the velocity components at x/H=5.0. Squares – experiment, Full line – numerical.

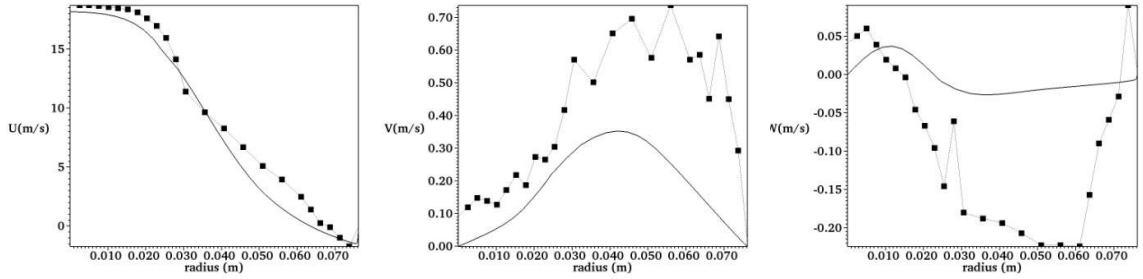

Figure 12. Results for the velocity components at x/H=6.0. Squares – experiment, Full line – numerical.

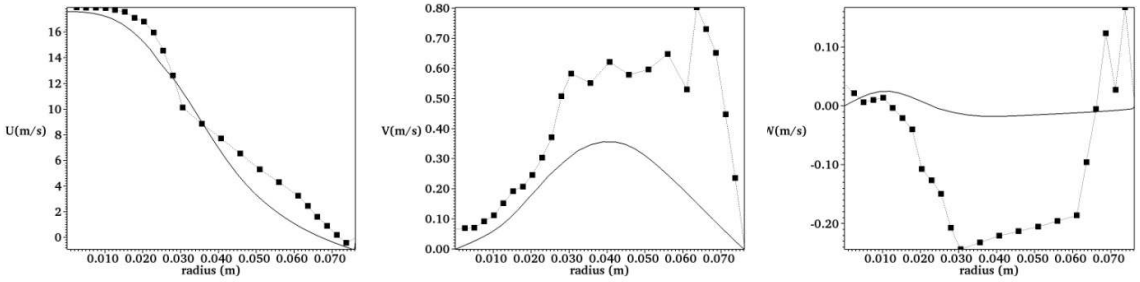

Figure 13. Results for the velocity components at x/H=8.0. Squares – experiment, Full line – numerical.

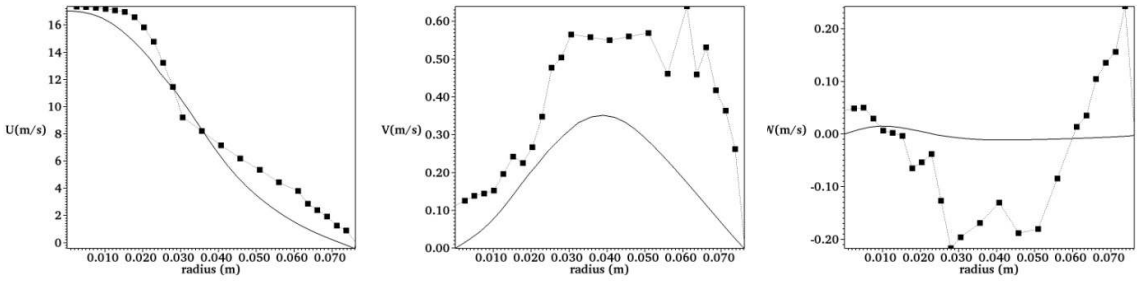

Figure 14. Results for the velocity components at x/H=10.0. Squares – experiment, Full line – numerical.

4.2. Results for S=0.4

Swirl is employed as a stabilization mechanism when handling large powers and inlet flow speeds. In these situations, the recirculation zone downstream of the sudden expansion, such as that when S=0, may not be sufficient to ensure flame stabilization (Poinsot and Veynante, 2005). The contours of the streamwise velocity in Fig. 15 clearly show the effects of the swirl on the streamwise velocity. Because of the centrifugal force, the profile of the axial velocity is bifurcating, yielding a low velocity zone along the chamber axis. The shift of the axial velocity has the purpose of causing flow recirculation close to the walls. The swirl can also be used to break liquid fuel jets. Nevertheless, the magnitude of the flow reversal with S=0.4 is lower than that of the nonswirling case, at least at the stations measured. The shear layers are also directed towards the walls by the rotation, as can be concluded by comparing Figs. 5 and 17. It is noticeable that, as the rotation weakens, nearly at x=0.20 m (Fig. 17), the shear layers tend to depart from the walls.

For high enough swirl numbers, the central recirculation zone may oscillate. This phenomenon is named precessing vortex core (PVC). Because these are steady-state and Reynolds-averaged simulations, phenomena like the PVC and vortex breakdown, which typically occur in rotating flows, cannot be detected or analyzed. LES would certainly serve this purpose, but the goal of this work is to assess the applicability of a RANS model to a high-Reynolds number flow at moderate swirl numbers. The SST model is routinely used to calculate flows at high Reynolds numbers with even higher swirl coefficients, such as those in internal combustion chambers. However, no assessment of the quality of the prediction in terms of flow dynamics, has been published.

Figures 18 to 20 present the radial profiles of the average velocity components for the swirling flow. The agreement between numerical and experimental results is good for the streamwise velocity close to the inlet, with decreasing agreement between experiment and simulation from x/H=4 on. The flow recirculation downstream of the swirler is predicted. Similar conclusions can be drawn for the swirling velocity component (W). A somewhat unexpected result is the overprediction of the swirling velocity in the core flow by the SST model. To the first author's best knowledge, RANS models normally underpredict swirl, as has been shown in a number of works on cyclone flows. However, it should be born in mind that the swirler is not being modeled, and the conclusions herein might be affected if it were included. It is also likely that the anisotropy of the flow, including the boundary layer region, might have to be taken into account by the turbulence model for reliable predictions, even under moderate swirl levels (0.4, as in this case). The magnitude of the radial velocity (V) is typically much lower than the others, and as such, difficult to measure and analyze critically.

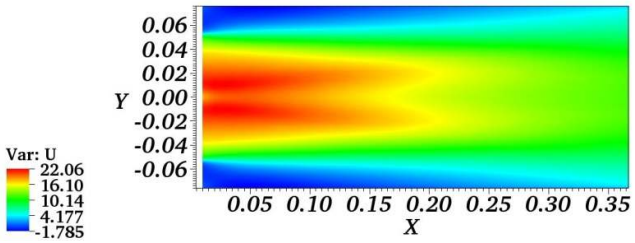

Figure 15. Contours of the streamwise velocity for S=0.4

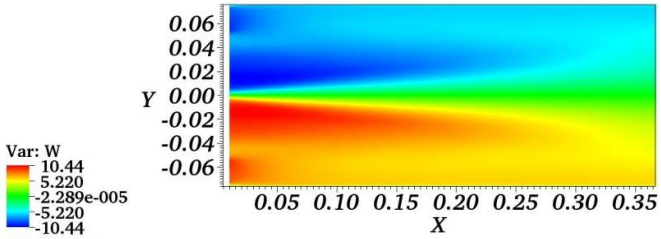

Figure 16. Contours of the swirling velocity for S=0.4

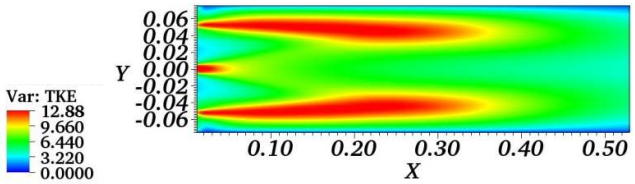

Figure 17. Contours of the turbulence kinetic energy for S=0.4

Regarding the experiments, one interesting feature is the substantial increase in swirl from the inlet (x/H=0.38) to the second measurement station (x/H=1.0). In the present situation, this effect is hard to be explained. As the flow enters the chamber, the only external forces it experiences are gravity and wall shear, and the latter tends to dissipate the swirl. By neglecting these forces, the angular momentum would have been preserved, as shown analytically by Heywood (1988), but not increased. Obviously, unless there is an external source in the momentum equations, no turbulence model can predict such increase in the swirling velocity. Aside from this abnormal effect, it can be seen that the swirling velocity decays more quickly than the model predicts. The same can be stated about the axial velocity.

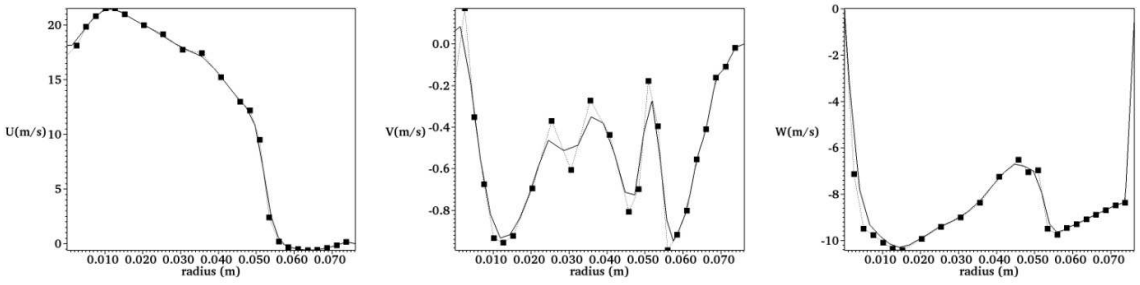

Figure 18. Results for the velocity components at x/H=0.38 (combustor inlet). Squares – experiment, Full line – numerical.

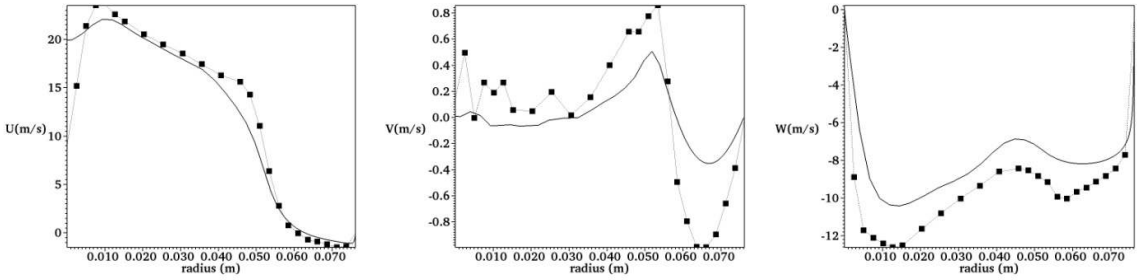

Figure 19. Results for the velocity components at x/H=1.0. Squares – experiment, Full line – numerical.

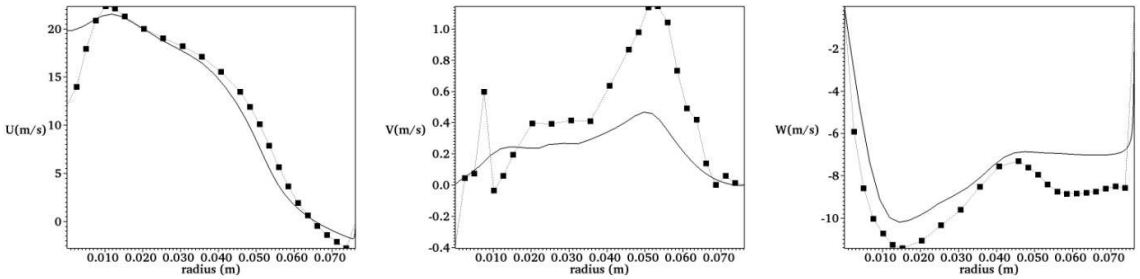

Figure 20. Results for the velocity components at x/H=2.0. Squares – experiment, Full line – numerical.

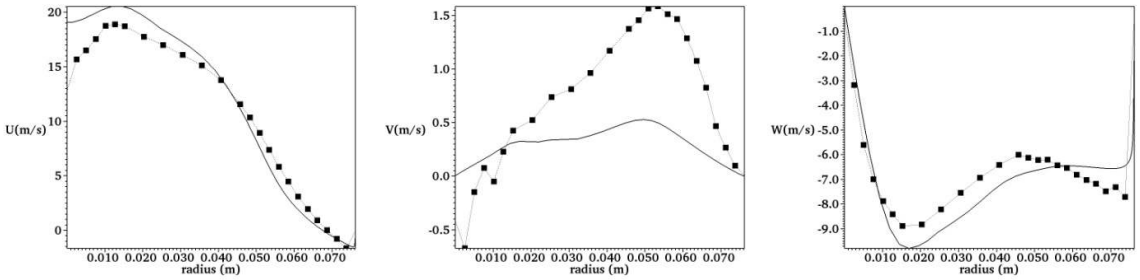

Figure 21. Results for the velocity components at x/H=3.0. Squares – experiment, Full line – numerical.

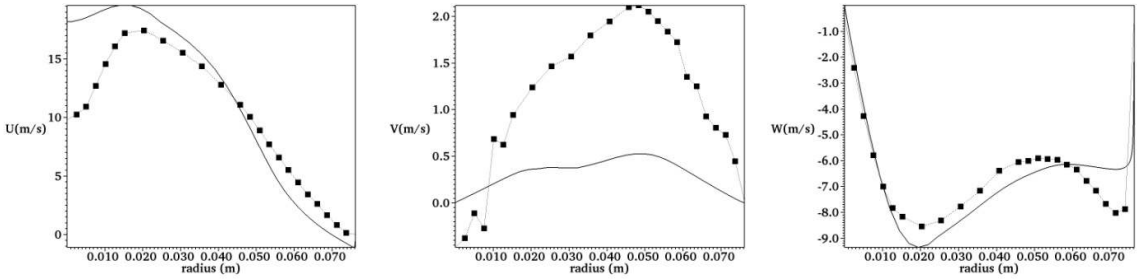

Figure 21. Results for the velocity components at x/H=4.0. Squares – experiment, Full line – numerical.

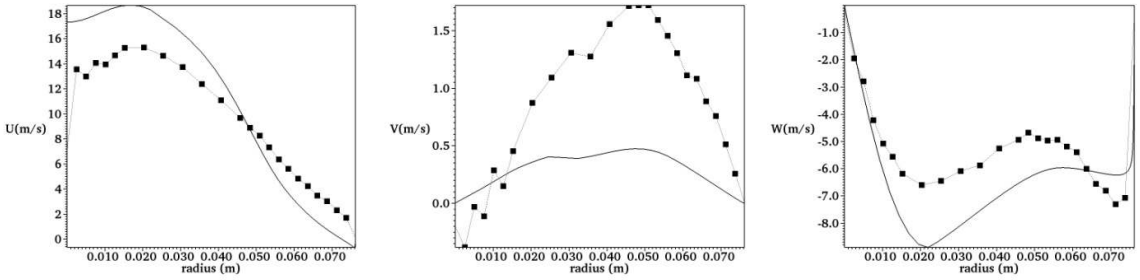

Figure 22. Results for the velocity components at x/H=5.0. Squares – experiment, Full line – numerical.

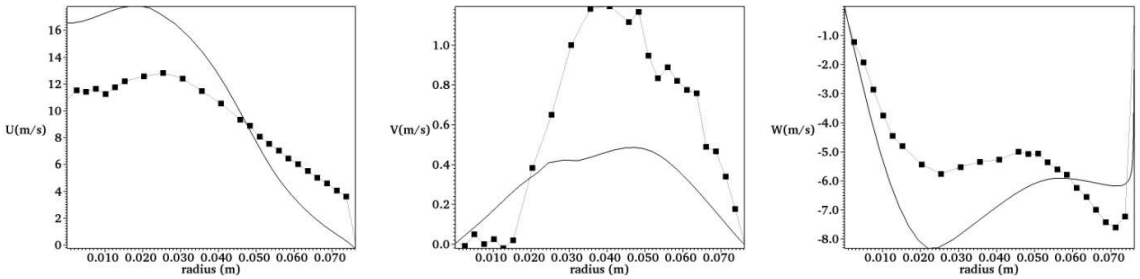

Figure 23. Results for the velocity components at x/H=6.0. Squares – experiment, Full line – numerical.

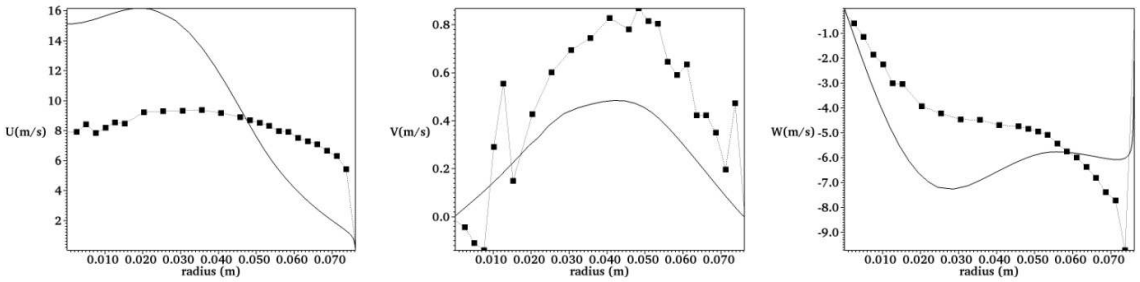

Figure 24. Results for the velocity components at x/H=8.0. Squares – experiment, Full line – numerical.

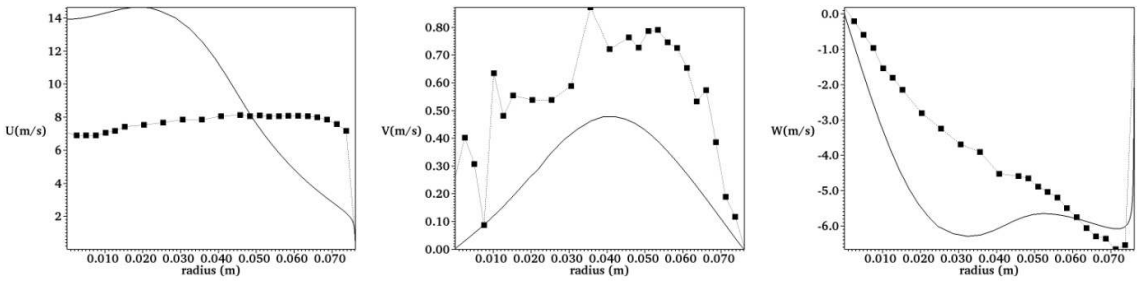

Figure 25. Results for the velocity components at x/H=10.0. Squares – experiment, Full line – numerical.

4.3. Results for S=0.4 with curvature correction

Figures 26 to 29 present the radial profiles of the average velocity components using the curvature correction in the SST model as proposed by Spalart and Shur (1997). Although this correction has been shown to provide good swirling velocity prediction in wing tip vortices and cyclone separator simulations (Menter, 2006), it can be seen that there is no improvement in the agreement between numerical and experimental results in this case. Actually, the swirling velocity is more overpredicted than that given by the standard SST model. Again, it should be emphasized that the inclusion of

the swirler might affect these findings, as in the situations where the curvature correction was successful (Menter, 2006), the mechanism for swirl generation was represented geometrically. Based on these and previous results, it can then be concluded that the turbulence viscosity provided by the turbulence model is not physically correct for this situation, a combustion chamber with prescribed swirl inlet profile. It is not obvious that a higher-order closure RANS model will improve results at this swirl intensity. Therefore, the swirler inclusion and an analysis of its impact on the swirling flow should be attempted before any further conclusions can be drawn.

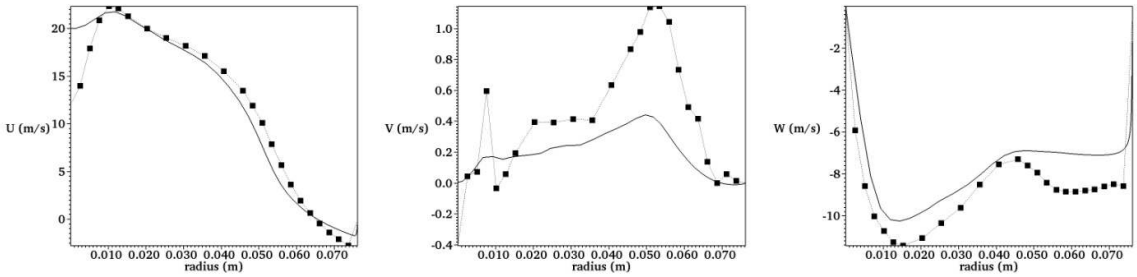

Figure 26. Results for the velocity components at x/H= 2 (SST model with curvature correction). Squares – experiment, Full line – numerical.

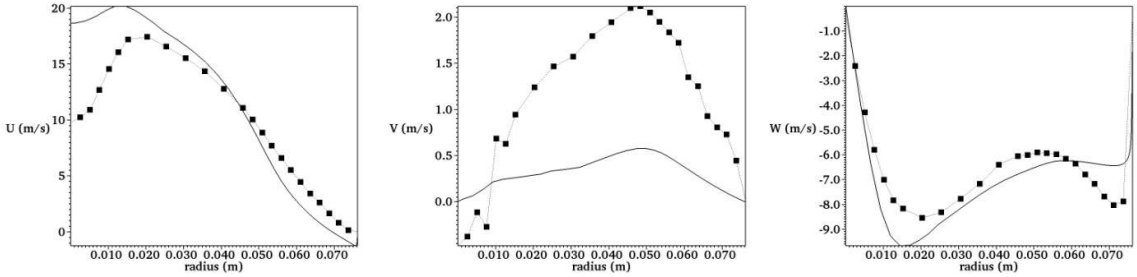

Figure 27. Results for the velocity components at x/H= 4 (SST model with curvature correction). Squares – experiment, Full line – numerical.

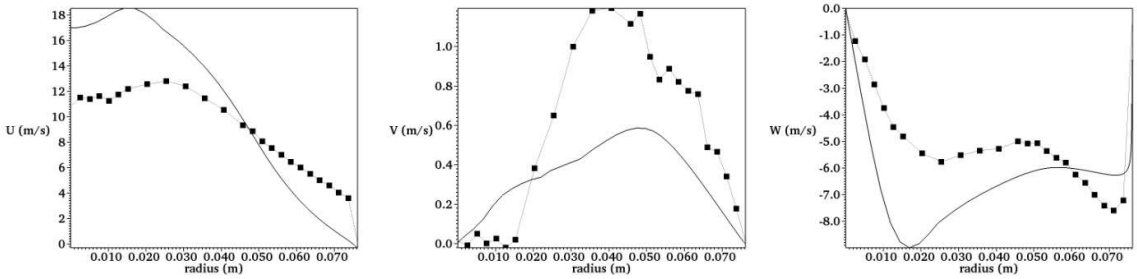

Figure 28. Results for the velocity components at x/H= 6 (SST model with curvature correction). Squares – experiment, Full line – numerical.

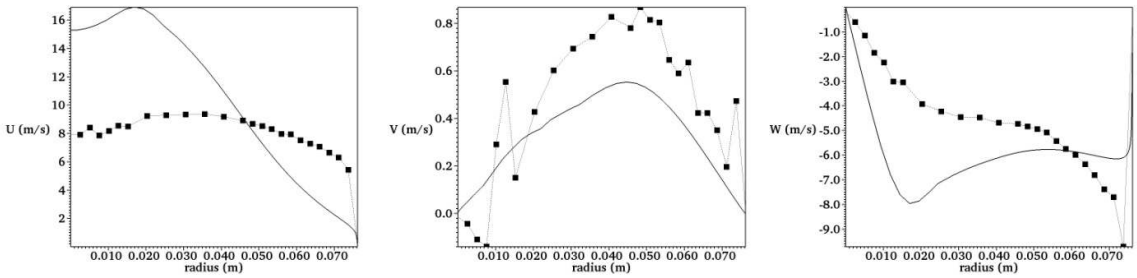

Figure 29. Results for the velocity components at x/H= 8 (SST model with curvature correction). Squares – experiment, Full line – numerical.

5. CONCLUSIONS

The cold, swirling and non-swirling flows in a dump combustor were simulated using the SST turbulence model and compared with experimental data. Results for the nonswirling case were found to be satisfactory, whereas the results for S=0.4 departed from the experiments, particularly far from the combustor inlet. Although this model is routinely used to calculate flows with even higher swirl coefficients, such as those in internal combustion chambers, it fails to predict the rotating flow in the dump combustor, at least in a model without a swirler. The curvature correction for the SST turbulence model proposed by Menter was evaluated and did not improve the agreement with experiments, despite successfully predicting other rotating flows. The swirler is not modeled and its inclusion may possibly improve results for the swirling flow.

6. REFERENCES

Ahmed, S. A., Nejad, A. S., 1992, "Velocity Measurements in a Research Combustor Part 1: Isothermal Swirling Flow", Journal of Experimental Thermal and Fluid Science, vol. 5 , pp.162 - 174.

ERCOFTAC – European Research Community on Flow, Turbulence and Combustion Database – Classic Collection. http://cfd.mace.manchester.ac.uk/ercoftac/classif.html

Ferziger, J. H. and Peric, M., 2002, "Computational Methods for Fluid Dynamics", Springer.

Heywood, J. B., 1988, "Internal Combustion Engines Fundamentals", McGraw-Hill.

Kim, S.-E., Mathur, S. R., Murthy, J. Y. and Choudhury, D., 1998, "A Reynolds-Averaged Navier-Stokes Solver Using Unstructured Mesh-Based Finite-Volume Scheme", AIAA-Paper 98-0231.

Langston, L. S. and Opdyke Jr., G., 1997, "Introduction to Gas Turbines for Non-Engineers", Global Gas Turbine News, v. 37, no 2.

Mathur, S. R. and Murthy, J. Y., 1997, "A Pressure-Based Method for Unstructured Meshes", *Numerical Heat Transfer*, vol. 31, pp. 195-215.

Menter, F. R., 1993, "Zonal Two-Equation k-ω Turbulence Model for Aerodynamic Flows", AIAA-Paper 1993-2906.

Menter, F. R., 1994, "Two-Equation Eddy-Viscosity Turbulence Models for Engineering Applications", AIAA Journal, 32 (8), pp.1598-1605.

Menter, F. R., 2006, "Introduction to Turbulence Modeling", course taught at ESSS, May 2006.

Poinsot, T. and Veynante, D., 2005, "Theoretical and Numerical Combustion", Edwards, 2nd edition.

Spalart, P. R. and Shur, M., 1997, "On the sensitization of turbulence models to rotation and curvature", Aerospace Sci. Tech., 1(5), pp.297-302.

7. RESPONSIBILITY NOTICE

The authors are the only responsible for the printed material included in this paper.